IEEE Photonics Journal
An IEEE Photonics Society Publication

Active Area Uniformity of InGaAs/InP Single-Photon Avalanche Diodes

Volume 3, Number 1, February 2011

A. Tosi
F. Acerbi
A. Dalla Mora
M. A. Itzler
X. Jiang

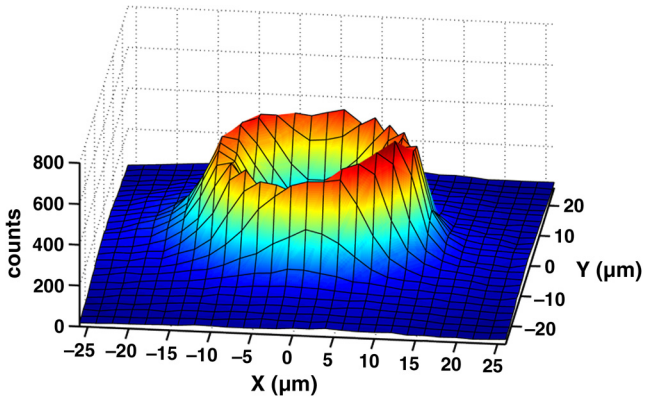

DOI: 10.1109/JPHOT.2010.2100037
1943-0655/$26.00 ©2010 IEEE

Active Area Uniformity of InGaAs/InP Single-Photon Avalanche Diodes

A. Tosi,[1] F. Acerbi,[1] A. Dalla Mora,[1] M. A. Itzler,[2] and X. Jiang[2]

[1]Dipartimento di Elettronica e Informazione, Politecnico di Milano, 20133 Milano, Italy
[2]Princeton Lightwave Inc., Cranbury, NJ 08512 USA

DOI: 10.1109/JPHOT.2010.2100037
1943-0655/$26.00 ©2010 IEEE

Manuscript received October 11, 2010; revised November 30, 2010; accepted December 8, 2010. Date of publication December 16, 2010; date of current version January 24, 2011. Corresponding author: A. Tosi (e-mail: alberto.tosi@polimi.it).

Abstract: We present a detailed characterization of the active area uniformity of InGaAs/InP Single-Photon Avalanche Diodes (SPADs) from two different design iterations. Nonuniformity of the electric field within the device active area has been measured through 2-D scans of detection efficiency and timing response to a pulsed laser. Additionally, we measured the near-infrared luminescence emitted by hot carriers during the avalanche. The nonuniformity is stronger at lower excess bias, with much higher and nonuniform electric field at the edge of the active area than expected, and it is fainter at higher excess bias, due to the saturation of the avalanche triggering efficiency. The main drawbacks are that the detection efficiency is position dependent when the SPAD is not fiber pigtailed and that the temporal response is worse, because of the nonuniform delay in the avalanche build-up across the SPAD active area.

Index Terms: Photodetectors, Single-Photon Avalanche Diodes (SPADs), photon counting, near-infrared detector, Avalanche Photodiode.

1. Introduction

Single-photon detectors are required in a wide range of applications in the near-infrared (NIR) range, i.e., between 1.0 and 1.7 μm, such as quantum cryptography [Quantum Key Distribution (QKD)] [1], Optical Time Domain Reflectometry (OTDR) [2], eye-safe laser ranging [LIght Detection And Ranging (LIDAR)] [3], Very-Large-Scale-Intergration circuit characterization based on light emission from hot carriers in metal–oxide–semiconductor field-effect transistors [4], singlet oxygen detection for dosimetry in PhotoDynamic Therapy (PDT) [5], time-resolved spectroscopy, etc.

Different technologies for single-photon detectors are available: PhotoMultiplier Tubes (PMTs), Superconducting Single-Photon Detectors (SSPDs), and Single-Photon Avalanche Diodes (SPADs). PMTs are broadly used and have wide active areas, but they have to be biased at high voltages and are bulky, fragile, and sensitive to magnetic fields. SSPDs have low noise and low time-jitter (30 ps) when operated at extreme cryogenic temperatures (2.4 K). SSPDs are capable of high count rates (in the gigahertz range), but the active area is small (typically 10 μm $\times$ 10 μm), and they require bulky cryostats.

SPADs offer the typical advantages of solid-state devices (small size, low bias voltage, low power consumption, ruggedness, and reliability) and fully exploit carrier multiplication when biased above breakdown [6]. When a single photon is absorbed, it triggers a self-sustaining avalanche, that is easily detectable by the read-out circuitry [7], which can be also easily integrated together with the silicon detector [8] and lead to large monolithic silicon SPAD arrays [9].

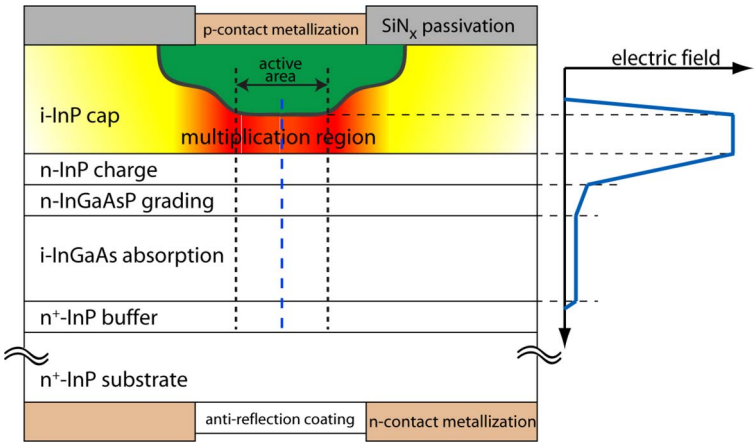

Fig. 1. Typical back-illuminated InGaAs/InP SPAD cross-section. Electric field in the multiplication region is sketched.

The main parameters that describe the performance of a SPAD are photon detection efficiency (PDE), dark count rate (DCR) (i.e., the noise), and timing jitter (i.e., the time spread between photon absorption and avalanche current build up, as read by the front-end electronics). Device designers have to optimize the internal structure in order to increase the detection efficiency while keeping both DCR and timing jitter low. PDE is the product of the absorption efficiency (i.e., the probability that an incident photon is absorbed) and the triggering efficiency (i.e., the probability that a photo-generated carrier ignites a self-sustaining avalanche). Both the triggering efficiency and the timing jitter depend on the electric field in the "multiplication" region, where carrier multiplication takes place, and they benefit from high electric fields. However, the DCR gets worse at high fields due to stronger tunneling effects that increase carrier generation. Therefore, the device design has to balance such different needs.

InGaAs/InP SPADs usually employ a Separate Absorption, Grading, Charge, and Multiplication (SAGCM) structure [10], with a double diffusion and floating guard rings (FGRs) in order to reduce edge effect of the electric field and to reach high fields only inside the active area. Moreover, those techniques efficiently reduce the surface leakage and enhance reliability.

In $In_{0.53}Ga_{0.47}As$/InP SPADs, the narrow band-gap of the infrared sensitive material provides high thermal carrier generation, and hence, the detector has to be cooled well below room temperature to keep the noise low. Thanks to recent improvements, low dark count rate is readily achievable, even with thermoelectric cooling systems.

In this paper, we describe the performances of commercially-available InGaAs/InP SPADs from two production runs. Our focus is the active area uniformity at different excess biases: We performed 2-D scans over the active area, and we measured the detection efficiency and the timing response to a pulsed laser. Additionally, we measured the near-infrared luminescence emitted by hot carriers during the avalanche. The results from the three methods highlight nonuniformity in the active area of the new generation SPADs, showing that the electric field is higher at the edge than in the center (due to nonoptimal suppression of edge effects) and that there is a general nonuniformity inside the active area.

2. Device Description

2.1. InGaAs/InP SPAD Structure

InGaAs/InP SPADs employ a SAGCM structure (see Fig. 1) [10]. A low-energy photon is absorbed in the InGaAs layer (Eg $\sim$ 0.75 eV at 295 K) and the generated electron-hole pair drifts thanks to the electric field. The hole enters into the high field region and triggers the impact ionization process within the InP multiplication layer (Eg $\sim$ 1.35 eV), thus giving rise to a self-sustaining avalanche

process. Between the absorption and the multiplication region, a charge layer allows the shaping of the electric field profile in order to have high field only in the InP multiplication region, while reducing it in the InGaAs absorbing region, thus lowering tunneling and field-assisted thermal carrier generation in the low band-gap layer.

Design criteria for SPADs (intended for operation in Geiger mode above breakdown) are different from those of Avalanche PhotoDiodes (APDs) (for operation in linear mode below breakdown). For example, similar ionization coefficients for holes and electrons is not an issue for SPADs; peripheral leakage, which contributes to dark current in APDs, is not multiplied, does not trigger the SPAD, and does not contribute to its DCR. Furthermore, SPADs are designed to operate above the breakdown voltage and at a low operating temperature (usually well below 0 °C).

The lateral boundaries of the active area are usually set by a double p-type diffusion, which is composed of a deeper diffusion that defines the active area, and a shallower one, with larger diameter that guarantees edge breakdown suppression and low peripheral leakage.

2.2. Active Area Uniformity

An important issue in the fabrication of InGaAs/InP SPADs is the electric field uniformity within the active region.

Nonuniformity was an issue also for APDs, giving differences in gain over the device area. Studies and measurements on the 2-D (2-D) gain profile and on the methods to suppress edge gain are reported in the literature [11]–[14].

Uniform response across the active area is also a key parameter for SPADs: either free-space or fiber coupled to the light source. Indeed, when no fiber is used, the response to photons impinging at different positions in the active area must be the same, in terms of both detection efficiency and temporal response; otherwise, strong distortions are present in the acquired optical waveforms. Uniformity is also important in fiber-coupled devices both when multimode fibers are employed and when mono-mode fibers are used and good temporal response is requested.

Ideally, with uniform electric fields across the active area, a carrier has the same triggering probability wherever it is photo-generated. Hence, the resulting photon detection efficiency should be the same everywhere inside the active area, while it should sharply decrease outside of it. Actually, there are edge effects (caused by the curvature of the p-n junction) that increase the electric field at the edge of the deep diffusion (i.e., of the active area) compared with the center, because the effect of double diffusion is not optimal. Moreover, tolerances in the manufacturing process generate localized maxima in the electric fields. Therefore, SPAD design should tailor the depth of the shallow diffusion in order to properly suppress edge effects; if it is too shallow, it is not efficient; if it is too deep, the breakdown voltage of such a peripheral area is too low and will be too similar to that of the active area.

3. Experimental Characterization

We characterized three different devices from Princeton Lightwave Inc. (PLI) [15] that are representative of two successive SPAD generations. SPAD1 and SPAD2 are two samples from newer production runs, whereas SPAD3 is from a previous generation, with a slightly different design. The devices have an active area diameter of 25 μm, a detection efficiency up to 30% (at 1550 nm), and a DCR of tens of thousands of counts per second (SPAD3, the previous generation) or a few thousand counts per second (SPAD1 and SPAD2, the latest generation) at 225 K, with 5 V of excess bias (V_{EX}).

During our characterization, we operated the SPADs in gated-mode by means of a passive-quenching circuit. When the device is kept off (T_{OFF} time interval), the SPAD bias is 0.5 V below the breakdown voltage, while when the SPAD is turned on (T_{ON} time interval), the SPAD is biased a few volts above breakdown.

3.1. Dark Count Rate

Fig. 2 compares the DCR of the three devices under test at different temperatures. The slope of the curves depends on the dominant "dark" carrier generation mechanism: Higher slope (about a

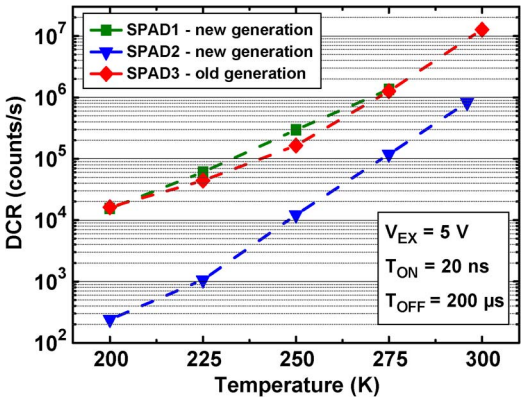

Fig. 2. Temperature dependence of the dark count rates for the three SPADs under test.

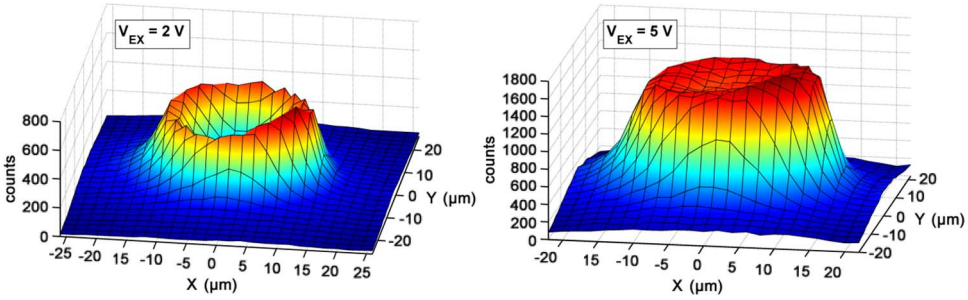

Fig. 3. Two-dimensional scans of SPAD1 at two excess bias, with the spatial dependence of photon detection efficiency at constant laser power. Relative changes in the photon counts represent the variation of the detection efficiency across the active area.

decade every 25 K) means thermal generation, while lower slope means tunneling generation (especially trap-assisted tunneling) [16]. The old generation device (SPAD3) has high DCR due to thermal generation at temperatures higher than 250 K and strong tunneling at temperatures lower than 225 K. New generation device SPAD2 shows a much lower DCR: The lower thermal generation is due to better material quality, and the lower tunneling generation is due to the designed lower electric field in the multiplication region. SPAD1 looks to be dominated by tunneling (only one slope for the entire temperature range), and its high DCR is due to poorer material quality that increased trap-assisted tunneling.

3.2. Photon Detection Efficiency

We performed a 2-D scan of the active area for assessing the uniformity of PDE (see Figs. 3–6). Data were obtained at 2 μm steps using a focused 1.55 μm laser with a 5-μm spot size on the SPAD active area. SPADs were operated in gated-mode with $T_{ON} = 20$ ns and a repetition rate of 20 kHz. The operating temperature was 225 K, and scans were taken at several values of excess bias. Since the laser power was kept constant (and at single-photon level) during the scan, the resulting maps (see Figs. 3–6) represent the variation of the detection efficiency across the SPAD area. In fact, the photon detection efficiency is given by the probability that a photon is absorbed multiplied by the probability that the photo-generated carrier triggers a self-sustaining avalanche.

Since the latter depends on the electric field, where the detection efficiency is higher, the electric field is there higher as well. Due to the curvature effect of the diffusion, higher electric fields are expected at the edge of active area (giving correspondingly higher detection efficiency in the maps of Figs. 3–6).

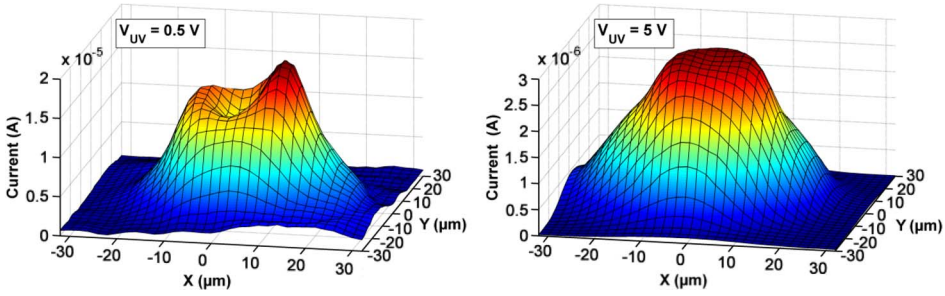

Fig. 4. Two-dimensional scan of the linear mode photocurrent of SPAD1 with the device biased at 0.5 V (left) and 5 V (right) below the breakdown voltage (UV meaning "under voltage").

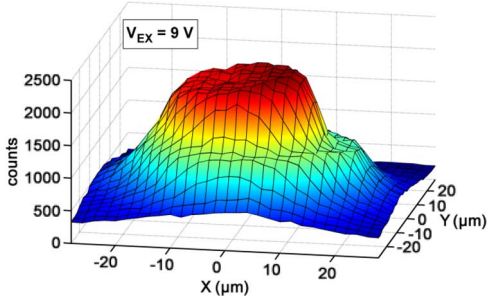

Fig. 5. Two-dimensional scans of SPAD1, with the spatial dependence of the photon detection efficiency at constant laser power.

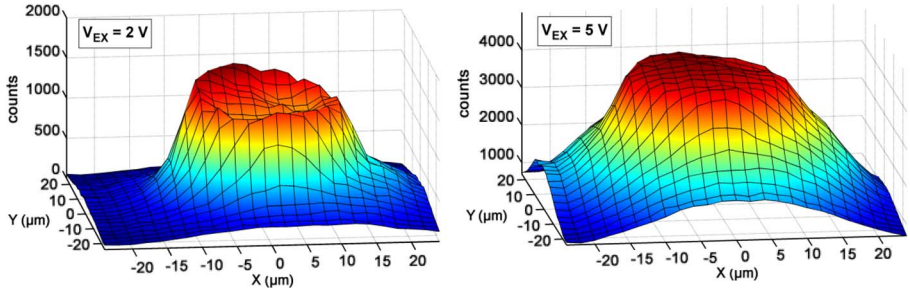

Fig. 6. Two-dimensional scans of SPAD2, with the spatial dependence of the photon detection efficiency at two excess biases.

Fig. 3 shows the PDE maps for SPAD1. The uniformity of this new generation device is very poor at low excess bias, with a much lower electric field in the center than at the edge of the active area. In detail, at $V_{EX} = 2$ V, SPAD1 can detect incident photons only along the circular ring at the edge of the central diffusion, while the center is almost insensitive.

At higher excess bias (5 V), the detection efficiency is more uniform, though not perfectly flat. The main cause is a problem encountered during the fabrication of this specific device run. The two consecutive diffusions of the double-diffusion process resulted in a larger difference between the deep (center) and the shallow (peripheral) diffusion depths than the intended design target. In order to adequately reduce edge effects of the electric fields, the central p-n junction has to be just slightly deeper than in the periphery. If the peripheral diffusion is too shallow with respect to the depth of the central region, then edge effects lead to enhancement of the electric field around the edge of the central region. (This situation is qualitatively similar to a junction formed by a single diffusion in

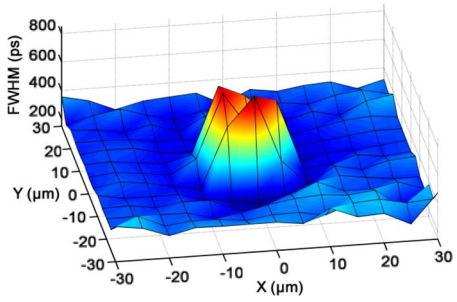

Fig. 7. Two-dimensional map of the FWHM of temporal response of SPAD1, with $V_{EX} = 3$ V.

which the peripheral region is entirely absent.) Additionally, it must be noted that the efficiency is not uniform along the edge or in the center because of the nonoptimal diffusion process. Such a Zn diffusion process is not well known and controlled as in similar processes employed for the fabrication of silicon devices. Therefore, the Zn diffusion depth can be nonuniform, giving to nonuniform electric field and triggering efficiency.

Similar scans of the linear mode gain below breakdown (see Fig. 4) show qualitatively similar edge peaking for this device, as expected. We measured the photocurrent that flows through SPAD1 while scanning the device at room temperature, at different bias from 5 V to 0.5 V under the breakdown voltage.

The device response gets progressively increasingly less uniform while getting closer to the breakdown voltage. At just 0.5 V below breakdown, part of the edge region reaches a 20% higher sensitivity than the central region.

We also measured the PDE at very high excess bias (9 V in Fig. 5). The uniformity in the active area improves while a new effect arises: Outside the nominal active area of 25 μm diameter, a surrounding area becomes photon sensitive. Such behavior arises from the peripheral area under the shallow diffusion, where the breakdown is low enough that at higher excess bias, this region also behaves like a SPAD.

Fig. 6 shows the 2-D scans of SPAD2 when measuring the spatial dependence of its PDE at constant laser power and at 225 K. Again, at low excess bias, the detection efficiency is less uniform than at higher excess bias. However, for this device, the nonuniformity is much lower than that found for SPAD1.

For SPAD2, the rise of PDE outside the nominal active area is present even at low excess bias ($V_{EX} = 2$ V, as visible in Fig. 7 for positive x value), thus producing a significantly wider photon-sensitive area at higher excess biases.

This is the same effect seen in Fig. 5 for SPAD1 but occurring at lower excess bias due to a value of the second (peripheral) breakdown that is closer to the first (center active area) breakdown.

3.3. Timing Jitter

Another important SPAD parameter is the timing jitter, which is measured by the Full-Width at Half Maximum (FWHM) of the arrival time distribution of photons due to a very sharp pulsed laser excitation. We measured the dependence of the timing jitter on the position where the SPAD is illuminated, and we reconstructed 2-D maps. The laser emits pulses at 1550 nm with a FWHM of less than 20 ps. The SPADs are cooled at 225 K, the light spot has a diameter of about 5 μm, and the scan is performed with steps of 5 μm over the SPAD active area.

The map at $V_{EX} = 3$ V of SPAD1 is shown in Fig. 7 and is in agreement with what was observed in the PDE characterization, i.e., at low excess bias, the SPAD central area has lower electric field, resulting in very poor timing response (i.e., FWHM is very large), while at the edge, the FWHM is narrower, indicating a larger electric field. Additionally, at higher excess bias (at least 5 V), the FWHM proved to be more uniform across the active area, similar to the detection efficiency behavior.

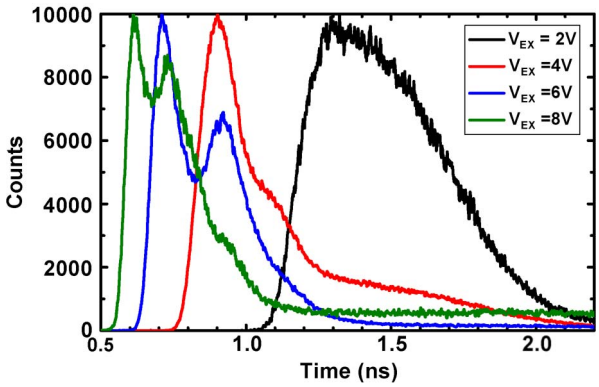

Fig. 8. Timing responses of SPAD2 to unfocused light at different excess bias (Normalized amplitudes).

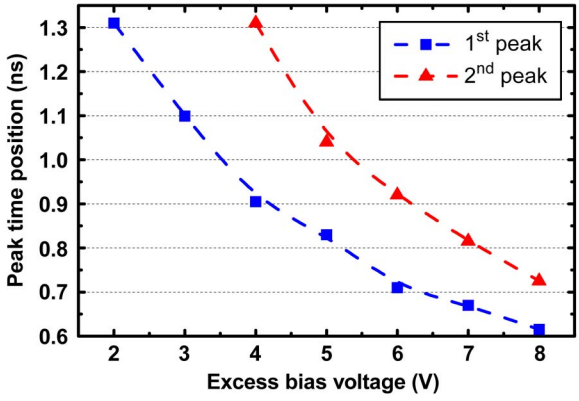

Fig. 9. Dependence of the two peaks time positions on excess bias, for SPAD2.

Concerning SPAD2, we first characterized the timing response by means of an un-focused light illumination so that the entire SPAD area was simultaneously illuminated with uniform power. The resulting timing response is composed of the superposition of the responses from all points of the SPAD. Fig. 8 shows different temporal responses of SPAD2 at different excess bias. The FWHM decreases at high excess bias, but at $V_{EX} > 4$ V, a second peak emerges. The time delay between the main and secondary peaks changes with excess bias. Fig. 9 shows the dependence of the time-position of the peaks on the excess bias: The two curves have the same trend, with just a 2-V shift. Therefore, the second peak originates from the edge of the device where the breakdown should be about 2 V higher than that of the central active area, which is in agreement with what was inferred from the photon detection efficiency maps.

The 2-D scans of timing jitter of SPAD2 show wide variations of both intensity and time position of the second peak, its amplitude at the edge being up to three times higher than the first peak. Moreover, when moving along the perimeter of the SPAD, there is a correlation between the intensity and the time shift: High second peak intensity corresponds to short shift and *vice versa*. This confirms that where the second breakdown is low, there is strong (high intensity) and prompt (short time shift) response to the light signal, even at the edge of the active area.

Fig. 10 shows different time response examples of SPAD2 when illuminated in the center of active area and in two points at the periphery where the second peak is evident. In the center, the second peak amplitude is always negligible.

Fig. 11 shows the map of the FWHM of the timing response. Higher value of the FWHM means wider response, due to a more delayed second peak, whereas lower value means that the two peaks are closer to each other or that the second peak has negligible amplitude.

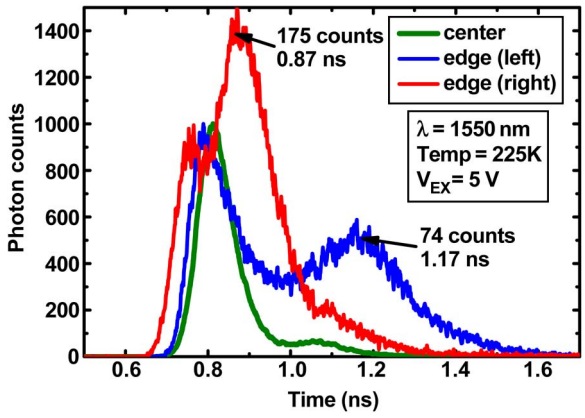

Fig. 10. Timing responses of SPAD2 with light focused. i) In the center of active area and ii) on the edge (in two points where the temporal response is different). (Curves are normalized to the amplitude of the first peak.)

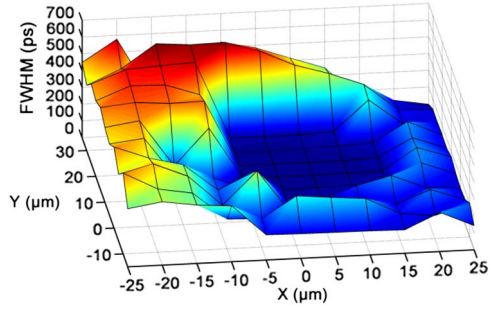

Fig. 11. Two-dimensional map of the FWHM of temporal response of SPAD2, with $V_{EX} = 5$ V.

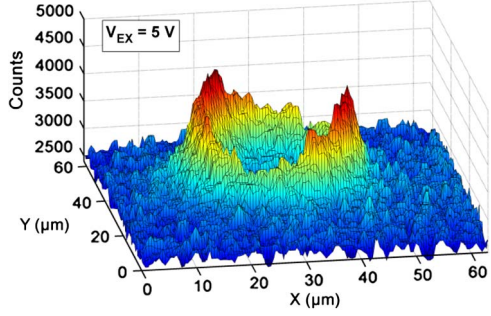

Fig. 12. Infrared photon emission due to hot-carriers from SPAD1, with $V_{EX} = 5$ V and working at 225 K.

At the device level, such behavior can be ascribed again to a nonuniform depth of the p-n junction in the periphery of the SPAD active area or by some other process nonuniformity (like diffusion mask misalignments). Probably, when the shallow diffusion is too deep, the resulting edge breakdown is too low and close to that of the central active area. Therefore, the depth of shallow junction must be precisely controlled in order to match the design specifications.

3.4. Infrared Emission

We measured the uniformity of the SPAD also by means of the intensity of the near-infrared luminescence emitted by the avalanching junction, due to hot carriers originating from the high

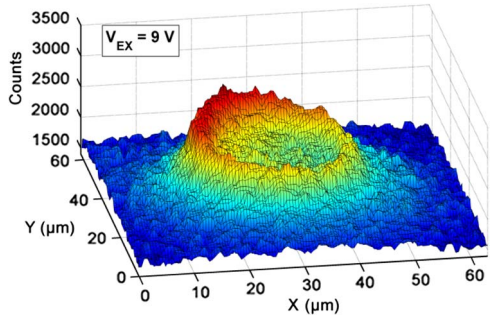

Fig. 13. Infrared photon emission due to hot-carriers from SPAD2, with $V_{EX} = 9$ V and working at 225 K.

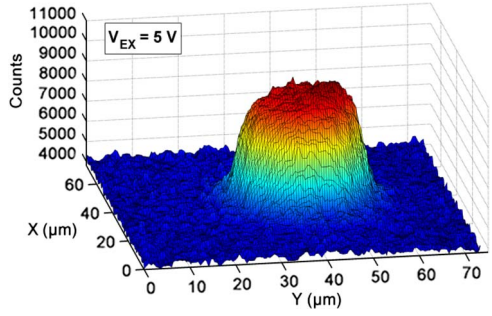

Fig. 14. Infrared photon emission due to hot-carriers from SPAD3, with $V_{EX} = 5$ V and working at room temperature.

electric field within the SPAD [17]. Those hot carriers are accelerated by the electric field; hence, the higher the field, the higher the carrier energy and the higher the emission intensity. We employed a scientific-grade silicon charged-coupled device camera (Hamamatsu C4880-21A) in order to collect the emission from the SPAD. Such measurements strongly highlight the electric field distribution because the photon emission probability depends almost exponentially on the electric field: Luminescence maps highlight slight differences in the electric field. Moreover, such a technique acquires the images at high spatial resolution and in a short time.

SPAD1 (see Fig. 12) and SPAD2 (Fig. 13) show high nonuniformity, with high electric field on the edge and with the edge itself being not uniform. At low excess bias, only one or two peaks at the edge are present. Increasing the excess bias, the electric fields at the edge becomes uniform. At higher excess bias, the electric field in the center is also quite high, thus decreasing the center-to-edge differences, as shown in Fig. 13. Additionally, for SPAD2, at very high excess bias, an increment in the electric fields at the periphery (outside) of the active area (i.e., under the shallow diffusion) is evident, which is in agreement with the 2-D scan of the detection efficiency. Therefore, in SPAD2 outside the nominal active area, the electric fields are high enough to trigger self-sustaining avalanches. Note that due to the exponential dependence of the infrared emission probability on the electric field, a direct comparison between measurements of the different techniques is not straightforward.

Finally, we characterized SPAD3 from the old generation. It shows very good edge-effect suppression with almost the same electric fields in the center and at the edge (see Fig. 14). The better suppression of the edge effect is due also to a smaller multiplication layer thickness. The smaller the thickness, the higher the electric fields in the center of the diffusion area with respect to the edge ones. The drawback is that the DCR is higher because of stronger tunneling.

We also measured the luminescence emission of an APD (model ETX40, manufactured at the former Epitaxx division of JDSU [18]) operated in Geiger mode. Such a detector has an active area diameter of 40 μm and the same basic structure shown in Fig. 1. Even in those samples, the emission is stronger on the edge of the active area due to electric field increase at the edge of the double diffusion, but it is fairly uniform both along the edge and inside the active area. Nevertheless, such devices were designed as linear-mode APDs, and the measured dark count rate in photon counting is much higher (hundreds of kilohertz) than that of those characterized here (a few kilohertz).

4. Conclusion

We characterized electric field uniformity of three commercially available InGaAs/InP SPADs from two production runs by means of three different methods. We performed 2-D scans of the detection efficiency and of the time response to a pulsed laser. Additionally, we measured the near-infrared luminescence emitted by hot carriers during the avalanche.

The results from the three methods are in a good agreement with each other and point out noticeable nonuniformity in the active area of the new generation SPADs. Detection efficiency is higher and timing response is narrower at the edge of the active area, especially at low excess bias. Therefore, the electric field is higher at the edge than in the center, due to nonoptimal suppression of edge effects, and there is a general nonuniformity inside the active area. Such strong nonuniformity is due to a nonoptimal control of the shallow peripheral diffusion depth, which produces much higher edge electric fields and gives local maxima in the electric field.

Since many SPAD parameters depend on electric field, poor uniformity gives poor performance, especially when the SPAD is either free-space coupled with the light source or coupled with multimode fibers (the presence of fiber speckles still requires uniform detectors). In fact, a different response to photons impinging in different points of the active area produces strong distortions in the acquired optical waveforms.

In order to counteract such distortions, the light should be focused in the center of active area to obtain stable and repeatable response. With an active area diameter of the present SPADs of 25 μm or more, it is feasible to focus the light in a small spot (less than 10 μm in diameter) in order to avoid distortions both in the detection efficiency and in the timing response. Unfortunately, to the best of our knowledge, nothing can be done on the read-out circuits connected to the SPAD in order to cope with the nonuniformity problem. We already employed in our characterization a circuit to read the avalanche signal with very low threshold, in order to be less dependent on the avalanche build-up statistics, but strong nonuniformity is still present, as previously shown.

On the device side, device manufacturers have to strive to better control the depth of the p diffusion. At the design level, SPAD designers have to conceive new solutions for making the electric field profile less sensitive to small changes in the junction depth. However, most of the job has to be done in the fab, where the p-type diffusion has to be better controlled because the double Zn diffusion process is still not completely reliable.

References

[1] H. Zbinden, H. Bechmann-Pasquinucci, N. Gisin, and G. Ribordy, "Quantum cryptography," *Appl. Phys. B*, vol. 67, pp. 743–748, May 1998.
[2] B. F. Levine, C. G. Bethea, and J. C. Campbell, "Room-temperature 1.3-μm optical time domain reflectometer using a photon counting InGaAs/InP avalanche detector," *Appl. Phys. Lett.*, vol. 46, no. 4, pp. 333–335, Feb. 1985.
[3] U. Schreiber and C. Werner, "Laser radar ranging and atmospheric LIDAR techniques," *Proc. SPIE*, vol. 3218, pp. 76–82, 1997.
[4] F. Stellari, A. Tosi, F. Zappa, and S. Cova, "CMOS circuit testing via time-resolved luminescence measurements and simulations," *IEEE Trans. Instrum. Meas.*, vol. 53, no. 1, pp. 163–169, Feb. 2004.
[5] M. J. Niedre, M. S. Patterson, A. Giles, and B. C. Wilson, "Imaging of photodynamically generated singlet oxygen luminescence in vivo," *Photochem. Photobiol.*, vol. 81, no. 4, pp. 941–943, Jul. 2005.
[6] H. Dautet, P. Deschamps, B. Dion, A. D. MacGregor, D. MacSween, R. J. McIntyre, C. Trottier, and P. P. Webb, "Photon counting techniques with silicon avalanche photodiodes," *Appl. Opt.*, vol. 32, no. 21, pp. 3894–3900, Jul. 1993.

[7] F. Zappa, S. Tisa, A. Tosi, and S. Cova, "Principles and features of single-photon avalanche diode arrays," *Sens. Actuators A, Phys.*, vol. 140, no. 1, pp. 103–112, Oct. 2007.
[8] F. Zappa, S. Tisa, A. Gulinatti, A. Gallivanoni, and S. Cova, "Complete single-photon counting and timing module in a microchip," *Opt. Lett.*, vol. 30, no. 11, pp. 1327–1329, Jun. 2005.
[9] F. Guerrieri, S. Tisa, A. Tosi, and F. Zappa, "Two-dimensional SPAD imaging camera for photon counting," *IEEE Photon. J.*, vol. 2, no. 5, pp. 759–774, Oct. 2010.
[10] M. A. Itzler, R. Ben-Michael, C. F. Hsu, K. Slomkowski, A. Tosi, S. Cova, F. Zappa, and R. Ispasoiu, "Single photon avalanche diodes (SPADs) for 1.5 μm photon counting applications," *J. Mod. Opt.*, vol. 54, no. 2, pp. 283–304, 2007.
[11] J. Burm, Y. Choi, S. R. Cho, M. D. Kim, S. K. Baek, D. Y. Rhee, B. O. Jeon, H. Y. Kang, and D. H. Jang, "Edge gain suppression of a planar-type InGaAs-InP avalanche photodiodes with thin multiplication layers for 10-Gb/s applications," *IEEE Photon. Technol. Lett.*, vol. 16, no. 7, pp. 1721–1723, Jul. 2004.
[12] Y. G. Xiao and M. J. Deen, "Modelling of two-dimensional gain profiles for InP-InGaAs avalanche photodiodes with a stochastic approach," *IEEE J. Quantum Electron.*, vol. 35, no. 12, pp. 1853–1862, Dec. 1999.
[13] J. N. Haralson, II, J. W. Parks, K. F. Brennan, W. Clark, and L. E. Tarof, "Numerical simulation of avalanche breakdown within InP-InGaAs SAGCM standoff avalanche photodiodes," *J. Lightw. Technol.*, vol. 15, no. 11, pp. 2137–2140, Nov. 1997.
[14] S. R. Cho, S. K. Yang, J. S. Ma, S. D. Lee, J. S. Yu, A. G. Choo, T. I. Kim, and J. Burm, "Suppression of avalanche multiplication at the periphery of diffused junction by floating guard rings in a planar InGaAs-InP avalanche photodiode," *IEEE Photon. Technol. Lett.*, vol. 12, no. 5, pp. 534–536, May 2000.
[15] Princeton Lightwave Inc. [Online]. Available: www.princetonlightwave.com
[16] M. Ghioni, A. Gulinatti, I. Rech, P. Maccagnani, and S. Cova, "Large-area low-jitter silicon single photon avalanche diodes," *Proc. SPIE*, vol. 6900, p. 690 01D, 2008.
[17] A. L. Lacaita, F. Zappa, S. Bigliardi, and M. Manfredi, "On the bremsstrahlung origin of hot-carrier-induced photons in silicon devices," *IEEE Trans. Electron Devices*, vol. 40, no. 3, pp. 577–582, Mar. 1993.
[18] M. A. Itzler, K. K. Loi, S. McCoy, N. Codd, and N. Komaba, "High-performance, manufacturable avalanche photodiodes for 10 Gb/s optical receivers," in *Proc. 25th OFC Conf.*, 2000, vol. 4, pp. 126–128.